AGU PUBLICATIONS

Geophysical Research Letters

RESEARCH LETTER
10.1002/2017GL074815

**Key Points:**
- The North Brazil Current system displays multidecadal variability
- This variability originates from the Southern Ocean
- The teleconnection is established through baroclinic Rossby waves

**Supporting Information:**
- Supporting Information S1

**Correspondence to:**
R. M. van Westen,
r.m.vanwesten@uu.nl

**Citation:**
van Westen, R. M., & Dijkstra, H. A. (2017). Southern Ocean origin of multidecadal variability in the North Brazil Current. *Geophysical Research Letters*, *44*. https://doi.org/10.1002/2017GL074815

Received 7 JUL 2017
Accepted 9 OCT 2017
Accepted article online 16 OCT 2017



# Southern Ocean Origin of Multidecadal Variability in the North Brazil Current

**René M. van Westen**[1] **and Henk A. Dijkstra**[1]

[1] Institute for Marine and Atmospheric Research Utrecht, Department of Physics and Astronomy, Utrecht University, Utrecht, Netherlands

**Abstract** Analysis of model data from a long (200 years) simulation of a high-resolution version of the Parallel Ocean Program indicates a connection between a mode of multidecadal variability in the Southern Ocean, the so-called Southern Ocean Mode, and multidecadal variability in the North Brazil Current. The multidecadal sea surface height variability in the Southern Ocean propagates northward and submerges at about 40°S. Northward propagating anomalies in ocean heat content are found between 5° and 40°S at depths down to 1 km and affect the North Brazil Current. Similar variability and connections between Southern Ocean and North Brazil Current are also found in a (200 years) simulation of a high-resolution global version of the Community Earth System Model. The results provide a new mechanism for the low-frequency variability of the North Brazil Current.

## 1. Introduction

Based on geostrophic transport time series, Zhang et al. (2011) find that the North Brazil Current (NBC) at 6°S displays pronounced (multi)decadal variability with peak-to-peak variations of about 7 sverdrup ($1\ \mathrm{Sv} \equiv 10^6\ \mathrm{m}^3\ \mathrm{s}^{-1}$). The cause of this long-term variability of the NBC transport has been linked to the Atlantic Meridional Overturning Circulation (AMOC). For example, Zhang et al. (2011) show an apparent correlation between the NBC transport time series and the formation of Labrador Sea Water. Further support for this connection comes from model studies, where significant correlations exist between the AMOC strength and the NBC transport (Wen et al., 2010; Rühs et al., 2015). Rühs et al. (2015) show that buoyancy-induced changes in the AMOC manifest themselves in the NBC, but that the variations are masked by strong interannual to decadal wind-driven gyre variability of the NBC.

As the northward NBC transport forms part of the AMOC upper branch, it is not surprising that NBC variations are well correlated to the 40°N AMOC strength (Zhang et al., 2011). However, it is less clear whether changes in the AMOC due to surface buoyancy changes in the Nordic Seas can lead to variations in the NBC transport. Certainly, low-resolution climate models show a large (and in phase) NBC response due to a collapse of the AMOC (Chang et al., 2008). However, the response in these models is much more coherent than that in high-resolution (near eddy-resolving) ocean models (Weijer et al., 2012). It is therefore highly uncertain whether relatively small variations in the AMOC (Smeed et al., 2014) can lead to a such a large NBC transport variability. In addition, it is suggested that the AMOC at 26°N displays a downward trend over the last decade (Smeed et al., 2014; Srokosz & Bryden, 2015). This is not directly compatible with the recent NBC transport observations at 11°S, which indicate that the mean NBC transport has not markedly changed over the period 2004–2014 (Hummels et al., 2015).

In this paper, we propose an alternative mechanism of the multidecadal variability of the NBC transport. Recently, Le Bars et al. (2016) identified the Southern Ocean Mode (SOM) in a multicentury simulation with the Parallel Ocean Program (POP, Smith et al., 2010). The SOM has a time scale of about 40–50 years and has a significant influence on the ocean heat content (OHC). As explained in Le Bars et al. (2016), the interaction between the large-scale ocean circulation and eddies is crucial (Berloff et al., 2007; Penduff et al., 2011) for the existence of the SOM and the mechanism can be understood from a three-layer quasi-geostrophic model (Hogg & Blundell, 2006). Indeed, Le Bars et al. (2016) do not find the SOM in a low-resolution (noneddying) version of their ocean model. The multidecadal variability that originates from the SOM also propagates northward (supporting information of Le Bars et al., 2016) into the Atlantic Ocean and affects the variability in the AMOC. Here we explore the connection between the SOM and NBC using data from the same multicentury

POP simulation as in Le Bars et al. (2016) as well as a new multicentury simulation with a high-resolution version of the Community Earth System Model (CESM, Hurrell et al., 2013).

## 2. Models Data and Methods

The 200 years of POP data are taken from the same control simulation as in Le Bars et al. (2016), and the output is available on a monthly resolution. The model has a 0.1° horizontal resolution on a curvilinear grid that captures the development and interaction of mesoscale eddies (Hallberg, 2013). For our analysis, we use the data that are transformed onto a rectangular grid with an approximate horizontal resolution of 0.4° × 0.4° and 42 nonequidistant depth layers. The model is forced under a (yearly) repeated seasonal mean, with further details provided elsewhere (Le Bars et al., 2016; Weijer et al., 2012). Below, the time series in POP are (linearly) detrended only if stated.

We also analyze data from a new 200 years CESM simulation, where the ocean component (the POP) and the sea-ice model have a 0.1° resolution. The number of vertical levels in the POP model is also 42. The atmosphere and land surface model have a horizontal resolution of 0.5°, and 30 nonequidistant pressure levels are used in the atmosphere model. The forcing conditions (e.g., $CO_2$, solar, and aerosols) are the observed ones over the year 2000 (repeated for every model year). The data (also transformed back onto a rectangular grid, similar to POP) analyzed have a monthly resolution. In the results below, all the analyzed time series from the CESM are (linearly) detrended.

As this is a recent CESM simulation, we present in the supporting information several time series that illustrate the equilibration of this simulation. Of course, the simulation time of 200 years is too short for equilibration of the AMOC and other deep ocean fields. However, the global mean surface temperature, the global mean sea surface temperature (SST), and radiative imbalance at the top of the atmosphere start equilibrating after about 150 years (Figures S1a and S1b in the supporting information) with only a small positive value of the global mean radiative imbalance over the last 50 years of the simulation. The Atlantic MOC strength at 1,200 m (Figure S1c) increases gradually and only shows a small trend at the end of the simulation. The upper ocean (700 m) heat content is still adjusting (Figure S1d), and stronger trends occur when heat content averages are taken over large depth. In the analysis of the CESM results below, we will take the last 131 years (years 70–200) of the simulation because the trends can easily be removed through linear detrending.

To analyze spatial-temporal variations of variability, for example, of the sea surface height (SSH) field, we use the Multichannel Singular Spectrum Analysis (M-SSA) (Ghil et al., 2002) technique, together with a Monte Carlo test (Allen & Robertson, 1996; Allen & Smith, 1996), to address significance. We follow the usual procedure (Schmeits & Dijkstra, 2000) where, for each time series, the linear trend and seasonal signal are first removed before a normalization (by the standard deviation). Next, a principal component analysis is applied to the resulting data and the number of principal components are retained to contain at least 90% of the total variance of the original time series. The significant periods found below using M-SSA did not change when a quadratic trend is removed from each time series instead of a linear one.

## 3. Results

### 3.1. NBC Transport Time Series

To represent the variability in the NBC, the westward transport in the NBC is averaged over the upper 700 m at 40°W and 50°W (Figure 1a). The latitudinal extent of the sections is approximately 13° and is based on the mean flow of the NBC and NBC return current. In the upper 700 m the NBC transport is directed westward (part of the AMOC upper branch), whereas at greater depths the Atlantic North Equatorial Undercurrent moves eastward. The mean SSH is taken over the NBC transport region (7°S–15°N; 48°–62°W), also indicated in Figure 1a. The raw time series of the NBC transport sections and SSH are (linearly) detrended over the analyzed period, the time mean is subtracted, and the result is smoothed through a running mean of 10 years.

In the POP results (Figure 2a), a clear multidecadal variability in SSH anomaly and NBC transport anomalies is seen, with a period of about 44 years. A lag correlation analysis indicates a significant correlation (95% confidence level, taking into account the reduction of the degrees of freedom due to the running mean), where the NBC transport anomalies are leading the SSH anomalies by about 5 years. In CESM (Figure 2b), there is clear multidecadal variability in both the NBC transport and SSH time series. However, the variability is less dominated by a particular period than in POP, and the NBC transport time series are more out of phase than in POP. The NBC transport anomalies are still leading the SSH anomalies, but the lag is less clear than in POP.

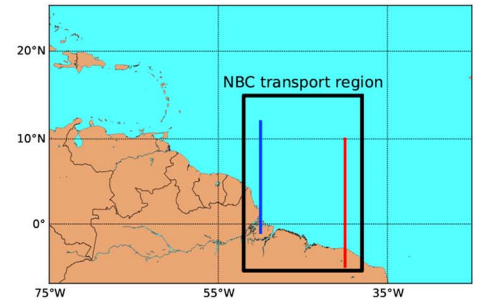


(a) Transport, SSH and OHC region

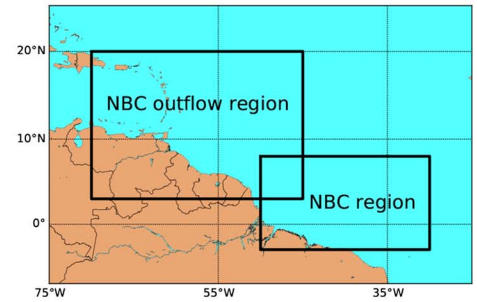


(b) M-SSA regions

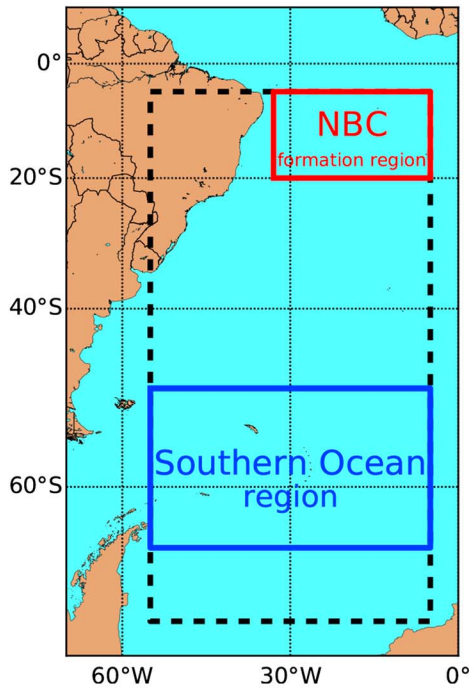


(c) OHC and Hovmöller region(s)

**Figure 1.** (a) Locations of the NBC transport sections, where red and blue are placed at 40°W and 50°W, respectively. The average SSH and OHC are determined in the NBC transport region restricted by the black box, over which also the M-SSA of SSH data is performed. (b) Two regions on which the M-SSA of SSH data is performed, named as the NBC region and NBC outflow region. (c) Two regions over which time series of the OHC is determined, the blue and red box are named the Southern Ocean region and the NBC formation region, respectively. Hovmöller diagrams of SSH and OHC are determined over the dashed region.

In the POP data, the AMOC strength (at 26°N and 1,200 m depth, Smeed et al., 2014), the NBC transport (at 6°S and averaged over the upper 1200 m, Zhang et al., 2011), and the SOM index (Le Bars et al., 2016) also display multidecadal variability (Figure S2a). The peak-to-peak variability in the NBC transport is 3 Sv and overall mean of about 25 Sv. The mean value is higher compared to reported values of NBC transport of approximately 16 Sv (Zhang et al., 2011, 1955–1996 mean at 6°S) and 22.1 $\pm$ 5.3 Sv (Schott et al., 2005, 1990–2004 mean at 5°S), but the variability is slightly lower.

The peak-to-peak variability in the AMOC is 2 Sv with an overall mean of about 19 Sv, comparable to reported values of 17.5 Sv (Smeed et al., 2014, 2004–2014 mean at 26°N). However, this observed mean could deviate from the actual volume transport value, as discussed in Hirschi and Marotzke (2007). In Le Bars et al. (2016) it was shown that the AMOC variability is caused by the SOM through northward propagation of density anomalies, and that its amplitude decreases northward. This is consistent with the results here, where the SOM leads the NBC transport by 26 years (312 months) and the NBC transport leads the AMOC by 4 years (53 months). In CESM (Figure S2b), the AMOC and NBC transports at 6°S display multidecadal variability and the overall mean is similar to POP: 18 Sv and 24 Sv, respectively. The peak-to-peak variability is slightly lower than in POP and is about 1 Sv for both quantities. There is no clear lag between the NBC transport and the AMOC, and also a lag correlation analysis between the SOM and the NBC transport time series provides no significant lag.

To study the dominant frequency of propagating patterns of multidecadal variability in the NBC transport region (Figure 1a), the SSH anomalies of this region are analyzed with M-SSA. In the POP SSH data, there is a significant variability in the NBC transport region with a period of 45–50 years (95% confidence interval) for a large range of lag-window lengths (between 620 and 800 months, see Table S1). The significance of this result is shown in Figure S3 using the Allen and Robertson (1996) test. For CESM, using the full length (200 years) of the SSH time series, we find a variability of 50 years in the NBC transport region, but it is not robust to the

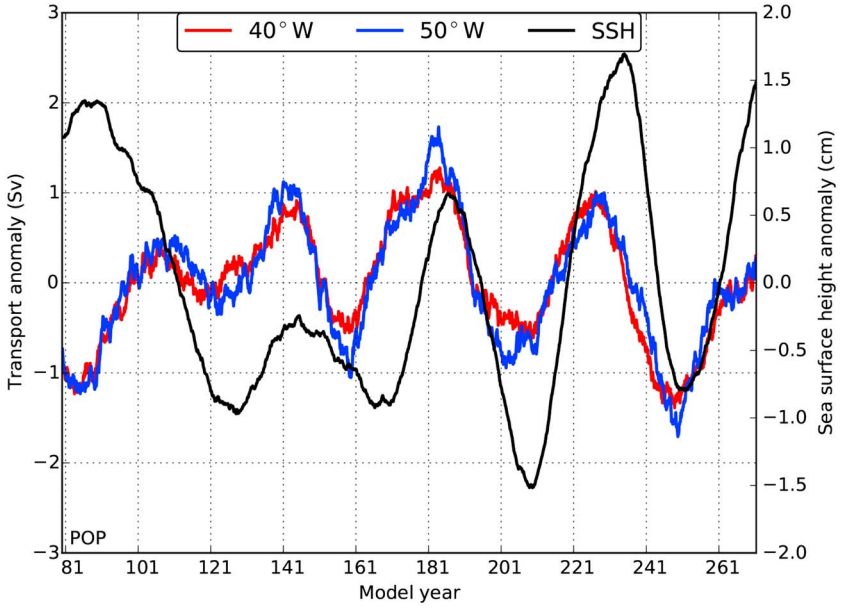


(a) POP

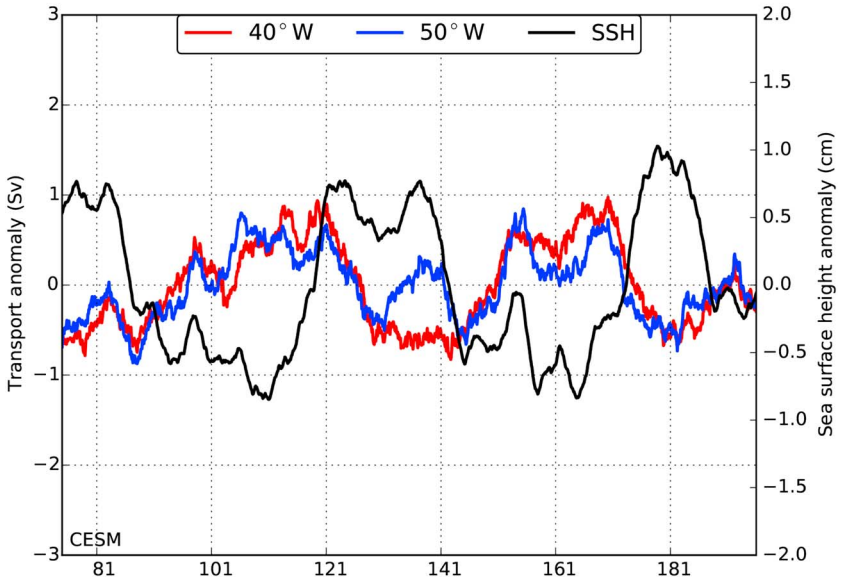


(b) CESM

**Figure 2.** Time series of the average SSH anomaly (black) and westward NBC transport anomalies at cross sections in the NBC transport region (see Figure 1a) for (a) POP and (b) CESM. All time series are (linearly) detrended, and the result is smoothed through a 10 year running mean.

lag-window length. However, the 45–50 year variability can be found (Tables S2 and S3) in the NBC region and the NBC outflow region (Figure 1b) for both models and is robust to the lag-window length.

### 3.2. SSH and OHC Anomaly Propagation

Hovmöller diagrams of SSH anomalies in the Atlantic Ocean are shown versus latitude for both POP and CESM in Figures 3a and 3b, respectively. For each month, we first determined the zonal mean SSH over 5°–55°W. Next, at each latitude, the time mean SSH of the monthly time series is subtracted to obtain anomalies, and these are smoothed through a 10 year running mean. The propagation velocity of the anomalies is determined along the axis of maximum amplitude of the anomalies.

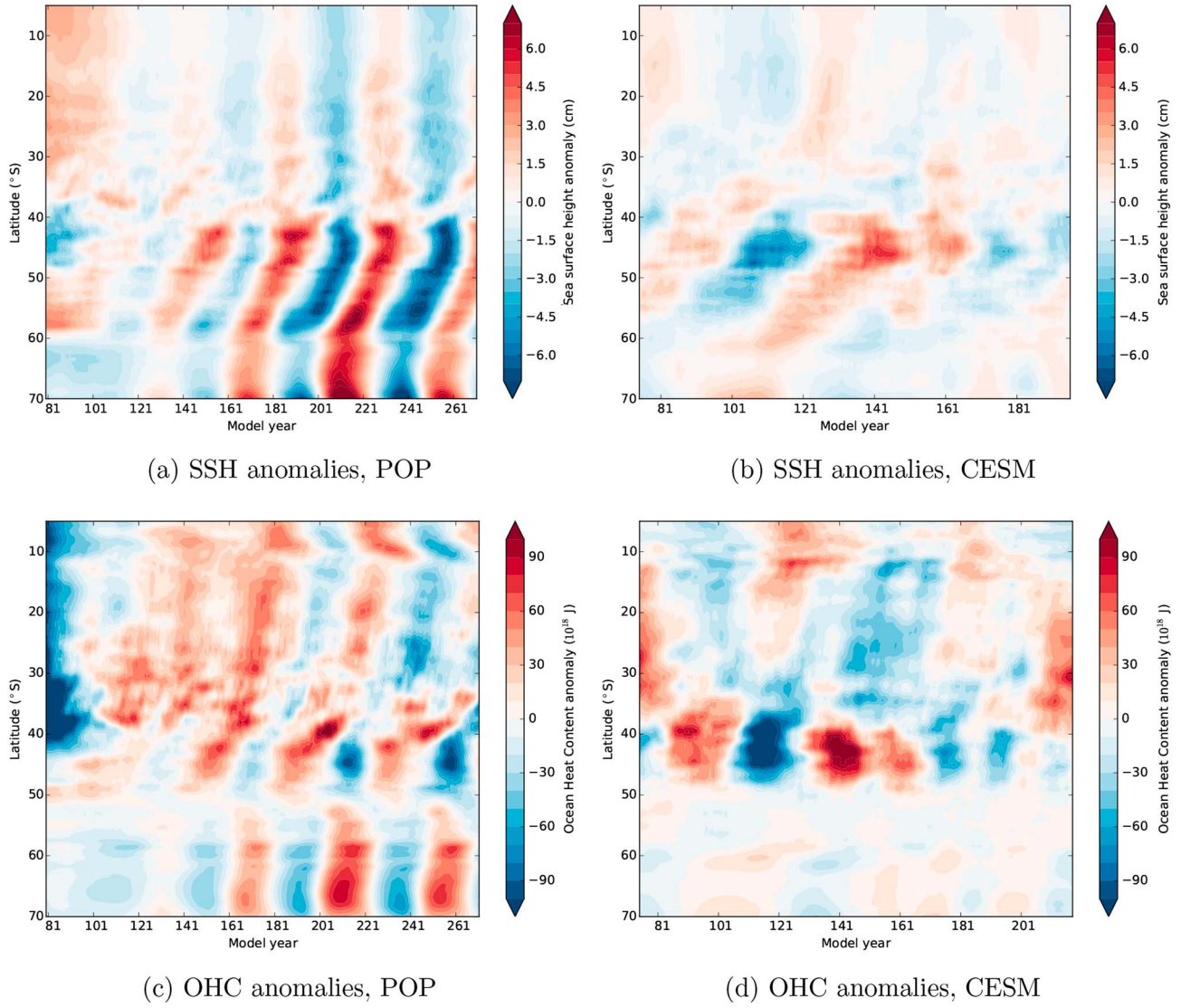


**Figure 3.** Hovmöller diagrams of SSH anomalies in (a) POP and (b) CESM along 5°W–55°W (see dashed box in Figure 1c). Hovmöller diagrams of OHC anomalies in the South Atlantic Ocean in (c) POP and (d) CESM. The OHC anomalies are averaged over 300–700 m and shown along 5°W–55°W. The data are smoothed through a running mean of 10 years.

In POP (Figure 3a) SSH anomalies propagate northward in the Southern Ocean (40°S–60°S) with a speed of about $73 \pm 3$ km yr$^{-1}$ and period of about 45 years. The SOM (Figure S2a) has the same period in the Southern Ocean, and therefore, this variability in SSH is associated with the SOM (Le Bars et al., 2016). The northward propagating anomalies strongly weaken at 40°S. Northward of 40°S, there are vertical bands of SSH anomalies, indicating that the anomalies become more stationary. The weakening of the SSH anomalies suggests that the anomalies from the Southern Ocean submerge near 40°S. In CESM (Figure 3b), SSH anomalies in the Southern Ocean (40°S–60°S) propagate northward with a speed of about $53 \pm 6$ km yr$^{-1}$. There are indications of multidecadal variability (for example, between model years 75–141), but the amplitude is much weaker compared to POP and the pattern much more localized. The SSH anomalies have the largest magnitude at 40°S and weaken as they propagate northward.

To investigate what happens near 40°S, Hovmöller diagrams of OHC are plotted in Figures 3c and 3d again both for POP and CESM, respectively. The OHC anomalies are averaged over depths of 300–700 m. The temperature, salinity, and pressure dependency of water density are taken into account when calculating the OHC (Millero & Chen, 1980). Although we also find multidecadal variability in the salinity fields between 300 and 700 m, the effect of haline contraction is smaller than thermal expansion, both on OHC and SSH

(steric effect) anomalies. In POP (Figure 3c), the OHC anomalies appear near 50°S in this part of the water column (300–700 m).

Together with information from the zonally averaged density profiles (Figure S4a), this indicates that density anomalies induced south of 40°S are submerged; they actually reach depths down to 1 km (see Figure S4b), but the center of the anomaly is located between 300 and 700 m. The OHC anomalies propagate northward from 50°S and reach 5°S (see Figures S4c and S4d) and even more northward latitudes (where they affect the AMOC), see Figure S5. Note that there is a phase difference between the OHC and overlying SSH anomalies between 5°S and 50°S, which depends on latitude. This phase difference is approximately 23 years (280 months) between 30°S and 40°S and decreases to 6 years (70 months) between 10°S and 20°S, where OHC leads SSH. These 6 years are similar to the phase lag found between the average SSH anomaly and the NBC transports (cf. Figure 2a) in the NBC transport region. Calculating the OHC anomalies over the upper 1 km leads to similar results.

In CESM, the OHC anomalies appear near 50°S, similar to those in POP and an irregularly oscillating pattern emerges as in the SSH anomalies (see Figure 3d), indicating that the variability is propagating northward and is submerged (Figure S6a). The positive (negative) OHC anomaly at 40°S in model year 100 (115) propagates northward (see Figures S6b–S6d). The patterns of northward propagating OHC anomalies is less clear compared to those in POP, but the propagation speeds are fairly similar (170 km $yr^{-1}$ for POP and 130 km $yr^{-1}$ for CESM over 250 months, Figures S4d and S6d). The phase difference between OHC and the overlying SSH anomaly at 30°S–40°S and 10°S–20°S is 23 years and 6 years, respectively, which is similar to POP.

Observations show a weak annual mean Ekman downwelling of 0–5 cm $d^{-1}$ near 40°S (Xie & Hsieh, 1995). In POP and CESM there is a mean Ekman downwelling of 2.9 and 4.4 cm $d^{-1}$ (spatial mean over 5°W–55°W; 40°S–50°S), respectively. The Ekman downwelling is weak and cannot explain why the OHC anomalies are also observed at 1 km below the surface. The OHC anomalies arise because the SOM leads to the displacement of isopycnals (see Figure S7) (Le Bars et al., 2016). The vertical displacement of the isopycnals excites baroclinic Rossby waves (Johnson & Marshall, 2002a) near 35°S. The average phase speed of OHC anomalies between 35°S and 10°S is about 197 ± 15 km $yr^{-1}$ and 128 ± 20 km $yr^{-1}$ for POP and CESM, respectively. When such a Rossby wave signal arrives at latitudes of the NBC, at least the baroclinic transport is affected causing changes in the NBC transport on multidecadal time scales.

Baroclinic Rossby waves are found in the interior (300–700 m) north of 30°S in the POP output (Figure S8a). Between 25°S–30°S, the average zonal phase speed of the Rossby waves is −6.0 cm $s^{-1}$. Theoretical values of a pure zonal ($l = 0$) linear propagating first-order baroclinic Rossby wave (derived from potential density profiles) is −7.6 cm $s^{-1}$. Rossby waves are also observed in the CESM output (see Figure S8b). The average zonal phase speed of the Rossby waves is −6.0 cm $s^{-1}$. Theoretical values of a pure zonal ($l = 0$) linear propagating first-order baroclinic Rossby wave (derived from potential density profiles in CESM) is −6.9 cm $s^{-1}$. Taking the meridional wavelength into consideration ($l \neq 0$) would lower the theoretical values for the propagation speed.

### 3.3. Teleconnection

To connect the OHC anomalies in the South Atlantic to the ones in the NBC formation region around 10°S, we also determined the OHC anomaly (averaged over 300–700 m) time series over the "Southern Ocean" region, the "NBC formation" region (Figure 1c), and the "NBC transport" region (Figure 1a). To better compare the time series, the NBC region values are scaled by $A_{SO}/A_{NBC}$, where $A_{SO}$ and $A_{NBC}$ are the areas for the Southern Ocean region and each NBC region, respectively. The results are shown in Figures 4a and 4b for both POP and CESM, respectively.

Again there is a clear multidecadal variability in each region in the POP data (Figure 4a). The OHC anomaly time series of the NBC formation region is lagging that from the Southern Ocean region by approximately 13 years (154 months). The variability from the NBC formation region reaches the NBC transport region within 1–4 years. Note that the scaled amplitude of the OHC anomaly in the NBC formation region and the NBC transport region is smaller compared to the Southern Ocean, indicating that the variability weakens while propagating northward (Johnson & Marshall, 2002a; 2002b). Indeed, Le Bars et al. (2016) show that the SOM temperature anomalies are distributed along the Antarctic Circumpolar Current and that their amplitude becomes smaller while moving northward. Determining the OHC anomalies over the upper 1 km gave similar results.

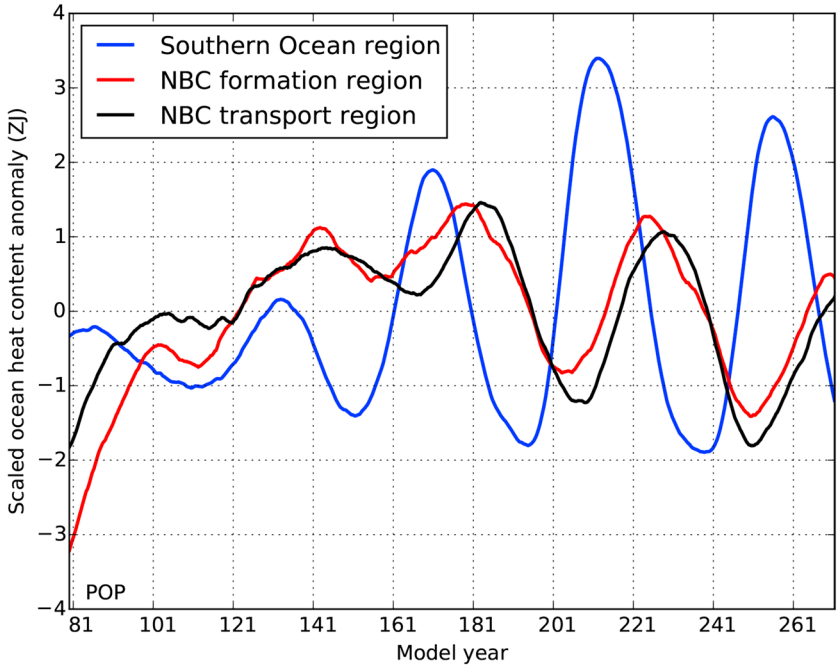


(a) POP

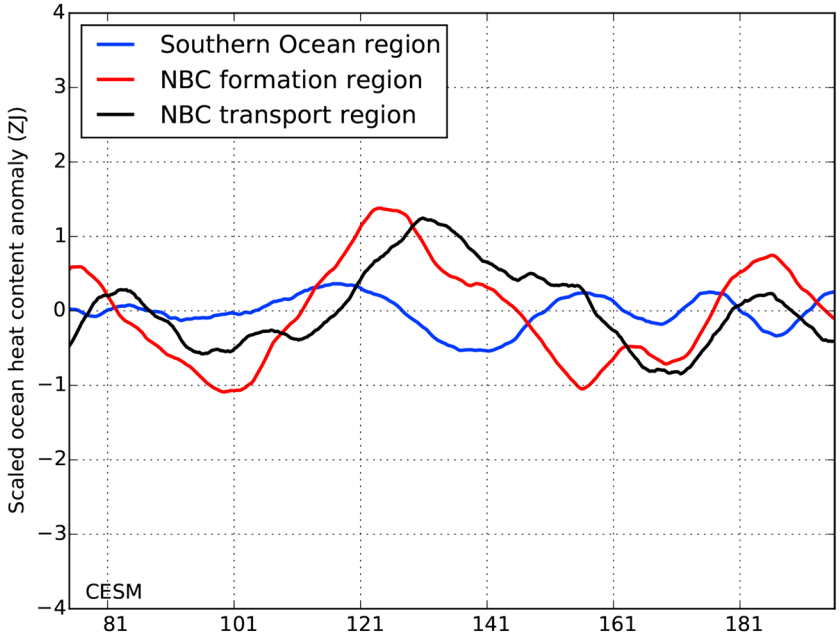


(b) CESM

**Figure 4.** Time series of OHC averaged over 300–700 m for (a) POP and (b) CESM for three regions: the Southern Ocean region, the NBC formation region, and the NBC transport region (Figure 1). The data are smoothed through a running mean of 10 years.

In the CESM results, there is also a lag of 12 years (143 months) between the OHC anomaly time series of the Southern Ocean region and that in the NBC formation region. The OHC anomaly time series of the NBC transport region lags that from the NBC formation region by 7 years (83 months), which is longer compared to POP. The scaled OHC anomaly amplitude of the Southern Ocean region is smaller than that of the NBC regions. The OHC anomalies of the Southern Ocean region have a smaller magnitude in CESM than in POP (see Figure 3), whereas at 40°S, the anomalies are of similar amplitude. The smaller amplitudes of the anomalies in CESM are most likely the effect of sea-ice interactions and/or atmospheric forcing, which are not represented in POP. Determining the OHC anomalies over the upper 1 km did not influence the results.

## 4. Summary and Discussion

In this paper, we analyzed 200 years of data from a control simulation (under seasonal mean forcing) of a high-resolution version of POP and a simulation with the CESM under a forcing of the year 2000. The M-SSA analysis of the POP and CESM output shows a significant variability with a corresponding period of 45–50 years in the NBC. Based on our model simulations and their analyses, we propose that the multidecadal variability in the NBC (Zhang et al., 2011) has a Southern Ocean origin and is associated with the SOM (Le Bars et al., 2016). Although the CESM simulation is shorter and still equilibrating, the results are important to demonstrate robustness of this SOM-NBC connection (as most clearly seen in the POP results) in the coupled ocean-atmosphere system.

In POP, the SSH anomalies due to the SOM are propagating northward with a speed of 73 km $yr^{-1}$. While the anomalies submerge at 40°S, the variability associated with the SOM can still be traced as subsurface temperature and hence OHC anomalies. Around 35°S, isopycnals are moved under the influence of the SOM, generating baroclinic Rossby waves. This different mechanism causes a change in propagation speed of OHC anomalies compared to the propagation of SSH anomalies in the Southern Ocean. In the South Atlantic Ocean (near 10°S), there is a phase difference of 70 months between OHC and SSH anomalies, where OHC leads SSH. This phase difference is also found between SSH and transport anomalies in the NBC. Both SSH and OHC anomalies have a Southern Ocean origin but have a different propagating mechanism. In CESM, the SOM can be distinguished and is weaker than in POP. However, the results of CESM show the same variability and teleconnection as in POP, and also the SSH and OHC anomalies can be traced from the Southern Ocean to the NBC region.

When the OHC anomalies reach the NBC formation region near 10°S, they can cross the equator and flow northward and affect the strength of the upper branch of the AMOC (Kuhlbrodt et al., 2007; Rahmstorf, 2002). In POP, due to near periodic changes in OHC in the NBC region, the NBC transport and consequently the AMOC also fluctuate with the same period as the SOM in agreement as shown in Le Bars et al. (2016). A consequence is that multidecadal AMOC variability would rather be a consequence of variability in the NBC than causing it, and hence, monitoring the NBC would not be very useful for detecting changes in the AMOC (Rühs et al., 2015). We hope that this work will stimulate further work on the possible SOM-NBC-AMOC connection.

**Acknowledgments**
The computations were done on the Cartesius at SURFsara in Amsterdam. Use of the Cartesius computing facilities was sponsored by the Netherlands Science Foundation (NWO) under the project SH-284. The data from the model simulations used in this work, as well as the analysis scripts, are available upon request from the authors.

## References

Allen, M. R., & Robertson, A. W. (1996). Distinguishing modulated oscillations from coloured noise in multivariate datasets. *Climate Dynamics*, *12*(11), 775–784.

Allen, M. R., & Smith, L. A. (1996). Monte Carlo SSA: Detecting irregular oscillations in the presence of colored noise. *Journal of Climate*, *9*(12), 3373–3404.

Berloff, P., Hogg, A. M. c., & Dewar, W. (2007). The turbulent oscillator: A mechanism of low-frequency variability of the wind-driven ocean gyres. *Journal of Physical Oceanography*, *37*(9), 2363–2386.

Chang, P., Zhang, R., Hazeleger, W., Wen, C., Wan, X., Ji, L., … Seidel, H. (2008). Oceanic link between abrupt changes in the North Atlantic Ocean and the African monsoon. *Nature Geoscience*, *1*(7), 444–448.

Ghil, M., Allen, M. R., Dettinger, M. D., Ide, K., Kondrashov, D., Mann, M. E., … Yiou, P. (2002). Advanced spectral methods for climatic time series. *Reviews of Geophysics*, *40*(1), 1003. https://doi.org/10.1029/2000RG000092

Hallberg, R. (2013). Using a resolution function to regulate parameterizations of oceanic mesoscale eddy effects. *Ocean Modelling*, *29*(72), 92–103.

Hirschi, J., & Marotzke, J. (2007). Reconstructing the meridional overturning circulation from boundary densities and the zonal wind stress. *Journal of Physical Oceanography*, *37*(3), 743–763.

Hogg, A. M., & Blundell, J. (2006). Interdecadal variability of the Southern Ocean. *Journal of Physical Oceanography*, *36*, 1626–1645.

Hummels, R., Brandt, P., Dengler, M., Fischer, J., Araujo, M., Veleda, D., & Durgadoo, J. V. (2015). Interannual to decadal changes in the western boundary circulation in the Atlantic at 11°S. *Geophysical Research Letters*, *42*, 7615–7622. https://doi.org/10.1002/2015GL065254

Hurrell, J. W., Holland, M. M., Gent, P. R., Ghan, S., Kay, J. E., Kusher, P. J., … Marshall, S. (2013). The Community Earth System Model: A framework for collaborative research. *Bulletin of the American Meteorological Society*, *94*(9), 1339–1360.

Johnson, H. L., & Marshall, D. P. (2002a). A theory for the surface Atlantic response to thermohaline variability. *Journal of Physical Oceanography*, *32*(4), 1121–1132.

Johnson, H. L., & Marshall, D. P. (2002b). Localization of abrupt change in the North Atlantic thermohaline circulation. *Geophysical Research Letters*, *29*(6), 7-1–7-4. https://doi.org/10.1029/2001GL014140

Kuhlbrodt, T., Griesel, A., Montoya, M., Levermann, A., Hofmann, M., & Rahmstorf, S. (2007). On the driving processes of the Atlantic Meridional Overturning Circulation. *Reviews of Geophysics*, *45*, RG2001. https://doi.org/10.1029/2004RG000166

Le Bars, D., Dijkstra, H. A., & Viebahn, J. P. (2016). A Southern Ocean Mode of multidecadal variability. *Geophysical Research Letters*, *43*, 2102–2110. https://doi.org/10.1002/2016GL068177

Millero, F., & Chen, C. (1980). A new high pressure equation of state for seawater. *Deep Sea Research Part A. Oceanographic Research Papers*, *27*(3–4), 255–264.

Penduff, T., Juza, M., Barnier, B., Zika, J., Dewar, W. K., Treguier, A.-M., … Audiffren, N. (2011). Sea level expression of intrinsic and forced ocean variabilities at interannual time scales. *Journal of Climate*, *24*(21), 5652–5670.

Rahmstorf, S. (2002). Ocean circulation and climate during the past 120,000 years. *Nature*, *419*(6903), 207–214.

Rühs, S., Getzlaff, K., Durgadoo, J. V., Biastoch, A., & Böning, C. W. (2015). On the suitability of North Brazil Current transport estimates for monitoring basin-scale AMOC changes. *Geophysical Research Letters*, *42*, 8072–8080. https://doi.org/10.1002/2015GL065695

Schmeits, M. J., & Dijkstra, H. A. (2000). Physics of the 9-Month variability in the Gulf Stream region: Combining data and dynamical systems analyses. *Journal of Physical Oceanography*, *30*(1995), 1967–1987.

Schott, F. A., Dengler, M., Rainer, Z., Stramma, L., Fischer, J., & Brandt, P. (2005). The shallow and deep western boundary circulation of the South Atlantic at 5–11 S. *Journal of Physical Oceanography*, *35*(11), 2031–2053.

Smeed, D. A., McCarthy, G. D., Cunningham, S. A., Frajka-Williams, E., Rayner, D., Johns, W. E., … Bryden, H. L. (2014). Observed decline of the Atlantic Meridional Overturning Circulation 2004–2012. *Ocean Science*, *10*(1), 29–38.

Smith, R. D., Jones, P., Briegleb, B., Bryan, F., Danabasoglu, G., Dennis, J., … Yeager, S. (2010). The Parallel Ocean Program (POP) reference manual: Ocean component of the Community Climate System Model (CCSM) and Community Earth System Model (CESM) (Tech. Rep. LAUR-10-01853, 141 pp.). Los Alamos, NM: Los Alamos National Laboratory. Retrieved from www.cesm.ucar.edu/models/cesm1.0/pop2/doc/sci/POPRefManual.pdf

Srokosz, M. A., & Bryden, H. L. (2015). Observing the Atlantic Meridional Overturning Circulation yields a decade of inevitable surprises. *Science*, *348*(6241), 1255575.

Weijer, W., Maltrud, M. E., Hecht, M. W., Dijkstra, H. A., & Kliphuis, M. A. (2012). Response of the Atlantic Ocean circulation to Greenland ice sheet melting in a strongly-eddying ocean model. *Geophysical Research Letters*, *39*, L09606. https://doi.org/10.1029/2012GL051611

Wen, C., Chang, P., & Saravanan, R. (2010). Effect of Atlantic Meridional Overturning Circulation changes on tropical Atlantic sea surface temperature variability: A 21/2-layer reduced-gravity ocean model study. *Journal of Climate*, *23*(2), 312–332.

Xie, L., & Hsieh, W. W. (1995). The global distribution of wind-induced upwelling. *Fisheries Oceanography*, *4*(1), 52–67.

Zhang, D., Msadek, R., McPhaden, M. J., & Delworth, T. (2011). Multidecadal variability of the North Brazil Current and its connection to the Atlantic Meridional Overturning Circulation. *Journal of Geophysical Research*, *116*, C04012. https://doi.org/10.1029/2010JC006812